UNIVERSITY OF CALIFORNIA SAN DIEGO

Diffusion of Run-and-Tumble Microswimmers in Porous Media

A thesis submitted in partial satisfaction of the
requirements for the degree
Master of Science

in

Engineering Sciences (Mechanical Engineering)

by

Can Yang

Committee in charge:

Professor David Saintillan, Chair
Professor Stefan Llewellyn Smith
Professor Padmini Rangamani

2020

The thesis of Can Yang is approved, and it is acceptable in quality and form for publication on microfilm and electronically:

_____

_____

_____

Chair

University of California San Diego

2020

TABLE OF CONTENTS

LIST OF FIGURES

ACKNOWLEDGEMENTS

I would like to acknowledge Prof. David Saintillan for his supervision on my thesis. It is his patient support that encouraged me and guided me to the right track.

I also would like to thank Achal Mahajan and Antoine Beringer for introducing me to the topic of this thesis.

In addition, I thank Jin Liang for her company during the darkest days of my life.

ABSTRACT OF THE THESIS

Diffusion of Run-and-Tumble Microswimmers in Porous Media

by

Can Yang

Master of Science in Engineering Sciences (Mechanical Engineering)

University of California San Diego, 2020

Professor David Saintillan, Chair

Microswimmers are objects that are able to propel themselves actively in fluid environments. The typical motion of bacteria such as *E. coli* can be described by the run-and-tumble model, which consists of successive relatively straight runs in conjunction with erratic changes of the swimming direction known as tumbles. The process of diffusion of microswimmers in porous media is crucial in many biological and environmental systems, and their motility is critical for processes such as bioinfection, bioremediation and biodegradation. In this thesis, the diffusion of microswimmers in porous media is studied numerically based on the run-and-tumble model. The results show that an increase in volume fraction of the obstacles comprising the porous medium leads to a decrease in effective long-time diffusivity. In cases where obstables are allowed to

overlap, the diffusivity drops even more dramatically with volume fraction than in the case of no overlap. The effect of varying the range of pillar dimensions is also studied. In the case of overlapping pillars, it is found that the diffusivity increases slightly when the domain is filled with larger pillars.

Chapter 1

Introduction

The observations of Brownian motion, which denotes the continuous random motion of microscopic immersed particles in solution, can be traced back to 17th century. In 1828, Robert Brown reported irregular oscillations of pollen particles. He also found that this motion is not restricted to organics or their products, as non-organic minerals and rocks are also subject to this type of motion. Brownian motion is caused by the continuous collisions of fluid molecules against immersed particles. In 1905, Albert Einstein showed that particles of any size, from microscopic molecules to those large enough to be observed macroscopically, are subjected to thermal fluctuations [1]. This thermal energy is the root cause of Brownian motion, and the random motion of particles subjected to that is called 'diffusion'. Unlike thermal fluctuations that having no preferred direction, external applied forces such as gravitational sedimentation, centrifugal acceleration or electrical fields can introduce bias in the direction of diffusion [2].

In contrast to passive Brownian particles, active particles are able to transform the energy extracted from external sources into work for self-propulsion. Examples include macroscopic objects such as fish, birds, and humans, or microscopic swimming organisms such as *Escherichia coli* (*E. coli*) and *Listeria*. For these swimmers, the mechanism of swimming depends strongly on Reynolds numbers, or the ratio between inertial forces and viscous forces. Fish swim at Reynolds

numbers of the order of 10^5 by taking advantage of inertia, while bacteria live in low Reynolds numbers of order 10^{-5} where thrust mainly results from viscous forces [2, 8, 9]. Under the condition of low Reynolds number, the Stokes flow equation suggests that swimming relies on non-time reversible processes, which suggests totally different hydrodynamics from that of the time-reversible swimming strategies at high Reynolds number, such as fish that propel themselves by reciprocal flapping [3].

The existence of biological swimmers is ubiquitous: bacteria and archaea habit extensively in the Ocean, soil, deep continental subsurface, upper oceanic sediment, deep oceanic subsurface, groundwater, wastewater, animals and plants, with a total population of about 1.2×10^{30} cells, and serve as a critical part in the carbon and nutrition cycling in the ecosytem [12, 13]. Besides environmental impacts, biological swimmers are also crucial for human activities. Spermatozoa travels through the female reproductive tract to reach the site of fertilization, wastewater treatment benefits from microorganisms by removing dissolved organic matters [14, 15, 17]. On the other hand, they can also cause human health issues: bacteria such as *E. coli* can cause urinary tract infections affecting 150 million people per year, and helicobacter pylori present in the human stomach can cause peptic ulcers and stomach cancer [16, 18].

Active swimmers are not limited to biological swimmers: artificial swimmers with sizes comparable to biological microswimmers are gaining attention, taking advantage of their potential in medical, health care, and drug delivery applications wtih minimal invasion and infection [19, 20]. Some of them have magnetically triggered flagellar filaments that mimic the swimming strategy of some of biological swimmers, while autophoretic bimetallic rods with no moving parts that propel themselves by electrochemical reactions [6, 7, 21].

The mechanism of swimming of *E. coli*, a rod-shapred biological microswimmer with flagellar filaments mounted on the sides of its body, has been extensively studied [4]. The swimming pattern of *E. coli* can be described by the 'Run-and-Tumble' model: runs, which are steady directed straight motions in a certain direction, alternate with tumbles, which are erratic

changes in the direction of swimming [5]. During the run stage, the flagella turn anticlockwise and group into a bundle, and the rotation of this helical filament generates thrust to push it forward; in the tumble stage, they rotate clockwise and comes apart, each of these flagella rotating individually and thereby changing the direction of swimming [2]. The trajectory of a run is not perfectly straight due to rotational diffusion, and its direction changes by approximately 27° on average [2]. Experimental tracking shows that the duration of runs and tumbles satisfy exponential distributions, with means of 1s and 0.1s respectively, and that the duration of individual runs are not correlated. For the direction of swimming, in the dilute aqueous solution, *E. coli* do have a preferred change in swimming direction of 68° on average, but this preferred direction is wiped off since the swimmer forgets its original orientation after a few tumbles [5]. In addition to flagellated bacteria such as *E. coli* and Salmonella, eukaryotic swimmers propel themselves by cilia, which are shorter than typical flagella with different beating patterns with so-called power and recovery strokes, unlike the sinusoidal bending waves observed in flagellated swimming [11].

Although the transport of bacteria in free medium has been well studied, their motility in complex heterogeneous media such as human tissues and soils still requires exploration. Swimming of active particles in periodic lattices [22] and through the interstices between closely packed hydrogel particles [23] have been analyzed in experiments. Computer simulations of microswimmers with circular orbits in 2D porous media were also reported [24]. In this thesis, we apply numerical simulations to analyze run-and-tumble dynamics of microswimmers in idealized porous media and elucidate how the geometry of the medium affects the long-time diffusion of the swimmers.

Chapter 2

Numerical Model

2.1 2D Domains with Non-Overlapping Pillars

The run-and-tumble dynamics of microswimmers in porous media is numerically simulated in two dimensions as follows. The porous medium is modelled as a periodic box consisting of pillars with circular shape as show in Figure 2.1. Circular pillars are generated randomly, with position $\boldsymbol{P} = (P_x, P_y) \in \mathbb{R}^2$, and radius $R \in [D_{min}, D_{max}]$. We enforce periodic boundary conditions: if a pillar overlaps with any of the boundaries, an additional image pillar will be added on the other side of the box (Figure 2.1). Pillars are not allowed to overlap with each other in this case, therefore any pillar that are generated by the algorithm will be removed it overlaps with any of the existing pillars.

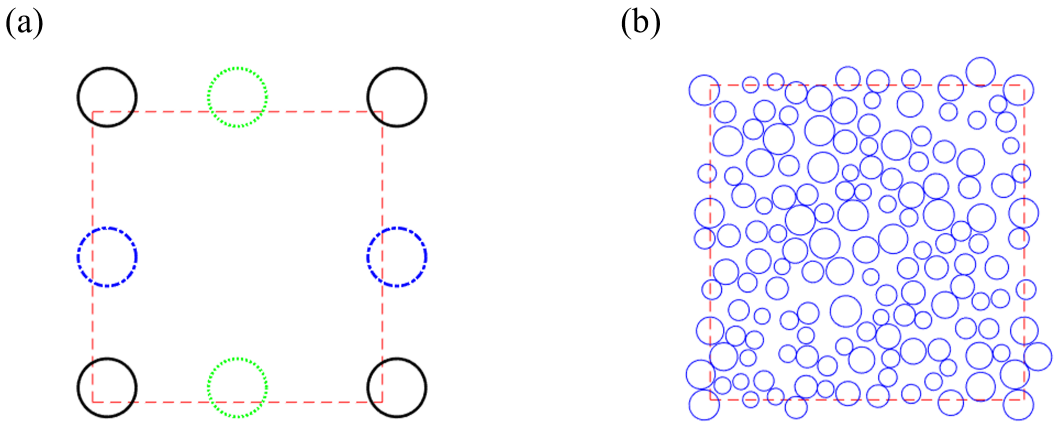

Figure 2.1: (a) Periodic boundary conditions. (b) Example of pillar distribution in a periodic box.

The volume fraction (or, to be precise, area fraction in two dimensions) is another factor that governs the porous medium geometry. It is defined as

$$\phi = \frac{V_{pillars}}{V_{box}} = \frac{\sum_{i=1}^{N} \frac{1}{4}\pi D_i^2}{L^2} \tag{2.1.0.1}$$

where N is the total number of pillars whose center is located inside the periodic box.

A swimmer is initially placed at the center of domain $\boldsymbol{S}_0 = \left(\frac{L}{2}, \frac{L}{2}\right)$. If the initial position of swimmer falls inside of a pillar, the swimmer will be shifted to the right until it is no longer inside the pillar. Once the swimmer is placed in the domain, the run-and-tumble model is applied to march time forward and update the position of swimmer. Swimmer transport is characterized by straight runs in certain direction and with a duration of run which is called the persistence time. Persistence times τ are extracted from an exponential distribution with mean of 1, and the swimming direction $\boldsymbol{p} = (cos(\beta), sin(\beta))$, which is characterized by angle $\beta(t) \in [0, 2\pi)$, is picked from uniform distribution. Since duration of tumble (0.1s) is much smaller than the

persistence time of a run (1s), the duration of tumbles is ignored in the simulation: between two runs, the swimmer orientation changes instantaneously.

More precisely, the simulations proceeds as explained here. At the beginning of each run, the swimming direction and duration are randomly selected. In the first place, we need to determine if collision with a pillar will take place (contact detection): If the particle does not collide with any of the pillars by the end of its run, the swimmer will move in a straight line throughout the current run, with final position $\boldsymbol{S}_i = \boldsymbol{S}_{i-1} + \tau \boldsymbol{p}$. However, if the swimmer collides with an obstacle during its straight run, we assume that the subsequent trajectory of the swimmer complies to the shape of pillar, i.e. swimmer will maintain its current orientation and will slide on the obstacle with the tangential component of its swimming velocity. To perform the contact detection, consider a particle located at an arbitrary position $\boldsymbol{S}_i$, with swimming direction $\boldsymbol{p}_i$. Pillars boundaries are defined by a group of second-order polynomials $(x-P_x)^2+(y-P_y)^2 = \frac{d^2}{4}$. Suppose that the swimmer will collide with a pillar during its run, then the position of the collision point is $\boldsymbol{S}_{collide} = \boldsymbol{S}_i + t_{collide}\boldsymbol{p}$ where $t_{collide}$ is unknown. To find it, we substitute $\boldsymbol{S}_{collide}$ into the equation of the circular pillar, solve the second order polynomial to obtain the time to collide. If there is no pillar located on the way of swimmer, the second order polynomial will return two imaginary roots; in this situation, swimmer will not collide with any of the pillars during this run.

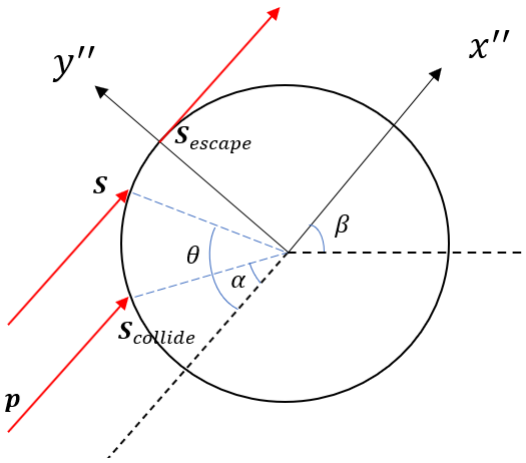

Figure 2.2: Setup of new coordinate system and angles

To determine swimmer motion after the collision, we define a new coordinate system $x''O''y''$ (Figure 2.2) with the origin at the center of pillar, the x axis aligned with the swimming direction of the current step, and the y axis satisfy right hand rule. α is the absolute angle between the negative x axis and the vector defined by the center of pillar and the collision point, θ is defined in similar manner but using the swimmer location after sliding instead of collision point:

$$\alpha = |Ang\,(\boldsymbol{S}_{collide} - \boldsymbol{P}_{collide}, -\boldsymbol{p})\,|, \tag{2.1.0.2}$$

$$\theta = |Ang\,(\boldsymbol{S} - \boldsymbol{P}_{collide}, -\boldsymbol{p})\,|. \tag{2.1.0.3}$$

At any instant of time, the swimmer will slide on the pillar with a tangential velocity of $\boldsymbol{v} = |\boldsymbol{v}_0|sin(\theta)$. It is clear that if α is 0 at the time of collision, the swimmer will just get stuck instead of sliding. Once the swimmer slides on the pillar, it can leave the pillar and proceed to swimming in a straight line again as $\boldsymbol{p}$ becomes tangent to the pillar ($\theta = \frac{\pi}{2}$) at its current location. It follows two scenarios: 1) The swimmer rests on the pillar at the end of its run; 2) The swimmer escapes from the pillar which it slides on. In the second case, once the swimmer escapes from the pillar, we must repeat the whole procedure described above (including contact detection with other pillars), with run time of $\tau - t_{collide} - t_{escape}$ while keeping $\boldsymbol{p}$ unchanged. Consequently, the time for the swimmer to escape from the pillar which it slides on should be computed in order to determine whether the swimmer will escape or not.

Consider a particle sliding on a pillar of diameter d. At any instant of time, its angular velocity along the pillar surface is given by:

$$\omega = \frac{d\theta}{dt} = \frac{|\boldsymbol{v}_0|\sin(\theta)}{d/2} \tag{2.1.0.4}$$

This can rearranged as

$$\frac{1}{|\boldsymbol{v}_0|\sin(\theta)} d\theta = \frac{2}{d} dt \tag{2.1.0.5}$$

$\theta = \alpha$ at the time of collision of the swimmer with the pillar, and the swimmer can escape as $\theta = \frac{\pi}{2}$. Therefore, to obtain the time taken for the swimmer to escape the pillar, we integrate θ from α to $\frac{\pi}{2}$ and time from 0 to t:

$$\int_0^{t_{escape}} \frac{2}{d} dt = \int_\alpha^{\frac{\pi}{2}} \frac{1}{|\boldsymbol{v}_0| \sin(\theta)} d\theta$$

$$\frac{2}{d} t_{escape} = \frac{1}{|\boldsymbol{v}_0|} log \frac{1/\tan\alpha + 1/\sin\alpha}{1/\tan\frac{\pi}{2} + 1/\sin\frac{\pi}{2}}$$

Rearranging yields the time for swimmer to escape from the pillar which it is sliding on:

$$t_{escape} = \frac{d}{2|\boldsymbol{v}_0|} \log\left(\frac{1}{\tan\alpha} + \frac{1}{\sin\alpha}\right) \tag{2.1.0.6}$$

We compare t given by (2.1.0.6) with the remaining time $t_{remain} = \tau_i - t_{collide}$ to determine whether the swimmer will escape from the pillar or not, where τ_i is run time for current step, $t_{collide}$ is the time for the swimmer to collide with the nearest pillar. If $t_{escape} > t_{remain}$, the swimmer leaves the pillar before the end of the current run; otherwise the swimmer will finish its run somewhere on the surface of the pillar.

Then next question is: if the remaining time is not enough for the swimmer to escape, where will it stop on the pillar? Starting from (2.1.0.5), we integrate over θ from α to θ_{end}, and time from 0 to t_{remain}:

$$\int_0^{t_{remain}} \frac{2}{d} dt = \int_\alpha^{\theta_{end}} \frac{1}{|\boldsymbol{v}_0| \sin\theta} d\theta$$

i.e.,

$$\begin{aligned}\frac{2|\boldsymbol{v}_0|}{d} t_{remain} &= -\log\left(\frac{\cos\theta_{end}}{\sin\theta_{end}} + \frac{1}{\sin\theta - end}\right) + \log\left(\frac{\cos\alpha}{\sin\alpha} + \frac{1}{\sin\alpha}\right) \\ &= \log\left(\frac{\frac{1}{\sin\alpha} + \frac{1}{\tan\alpha}}{\frac{1+\cos\theta_{end}}{\sin\theta_{end}}}\right)\end{aligned}$$

Take the exponential on both sides,

$$e^{\frac{2|\boldsymbol{v}_0|}{d}t_{remain}} = \frac{\frac{1}{\sin\alpha}+\frac{1}{\tan\alpha}}{\frac{1+c\theta_{end}}{\sin\theta_{end}}} \tag{2.1.0.7}$$

Define

$$A = \frac{\frac{1}{\sin\alpha}+\frac{1}{\tan\alpha}}{e^{\frac{2|\boldsymbol{v}_0|}{d}t_{remain}}}$$

Then (2.1.0.7) becomes

$$\frac{1+\cos\theta_{end}}{\sin\theta_{end}} = A$$

$$\theta_{end} = 2|\boldsymbol{v}_0|\tan^{-1}\frac{1}{A} \tag{2.1.0.8}$$

Since α, d and t_{remain} are all known, A is known for current step. Therefore, the position where the swimmer will be at the end of the time step is fully described by θ_{end}. Let $\boldsymbol{S}''_{collide}$ be the position of collision point with respect to $x''O''y''$, which is given by:

$$\boldsymbol{S}''_{collide} = \boldsymbol{R}(\boldsymbol{S}_{collide} - \boldsymbol{P}_{collide}) \tag{2.1.0.9}$$

where $\boldsymbol{P}_{collide}$ is the position vector of the collision point with respect to the initial coordinate system, i.e. $\boldsymbol{P}_{collide} = \overrightarrow{OP}_{collide}$. $\boldsymbol{R}$ is the rotation matrix$\boldsymbol{R} = \begin{bmatrix} cos\beta & sin\beta \\ -sin\beta & cos\beta \end{bmatrix}$. θ_{end} is the angle with respect to the relocated and rotated coordinate system $x''O''y''$. To obtain the position of swimmer with respect to the original coordinate system, we need to transfer the position information given by θ_{end} back to that coordinate frame:

$$\boldsymbol{S}_{end} = \boldsymbol{R}^{-1}\boldsymbol{S}''_{collide} - \boldsymbol{P}_{collide} \tag{2.1.0.10}$$

Note that for the case of escape, (2.1.0.10) could also be used to compute the point of escape by replacing θ with $[0, \frac{d}{2}]^T$, and $\boldsymbol{S}_{collide}$ by $\boldsymbol{S}_{escape}$, Where sign is the sign of the y component of

$\boldsymbol{S}''_{collide}$.

Overall, the steps described above can be summarized in the flow chart below in Figure 2.4.

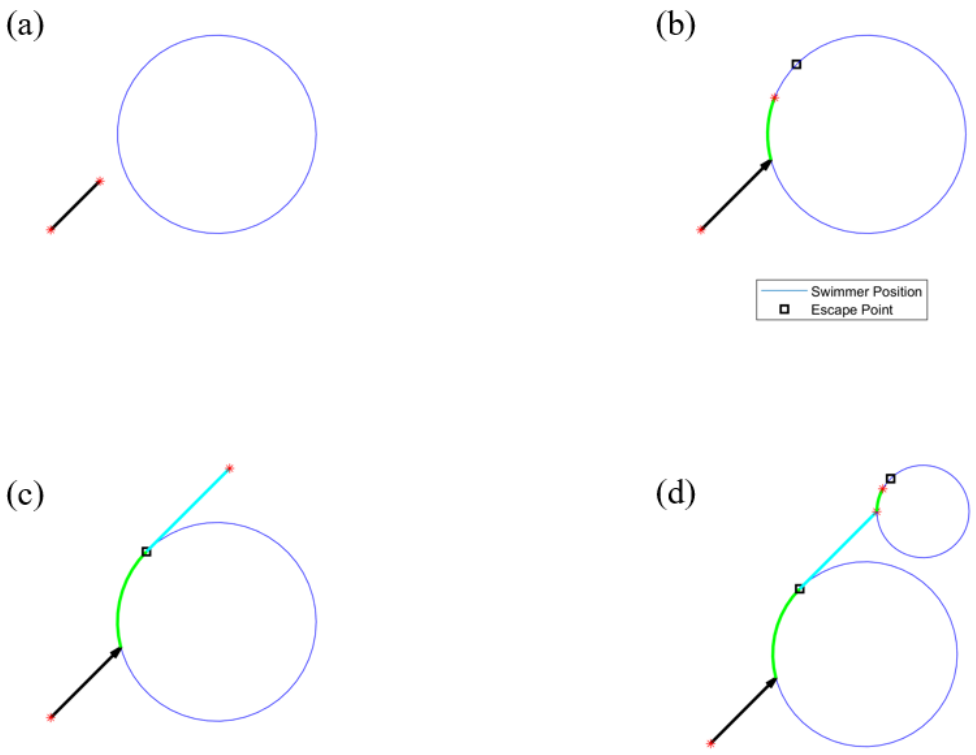

Figure 2.3: (a) No Collision. (b) Collision but no escape. (c) Collision and escape. (d) Collision, escape, and collision with another pillar after the escape.

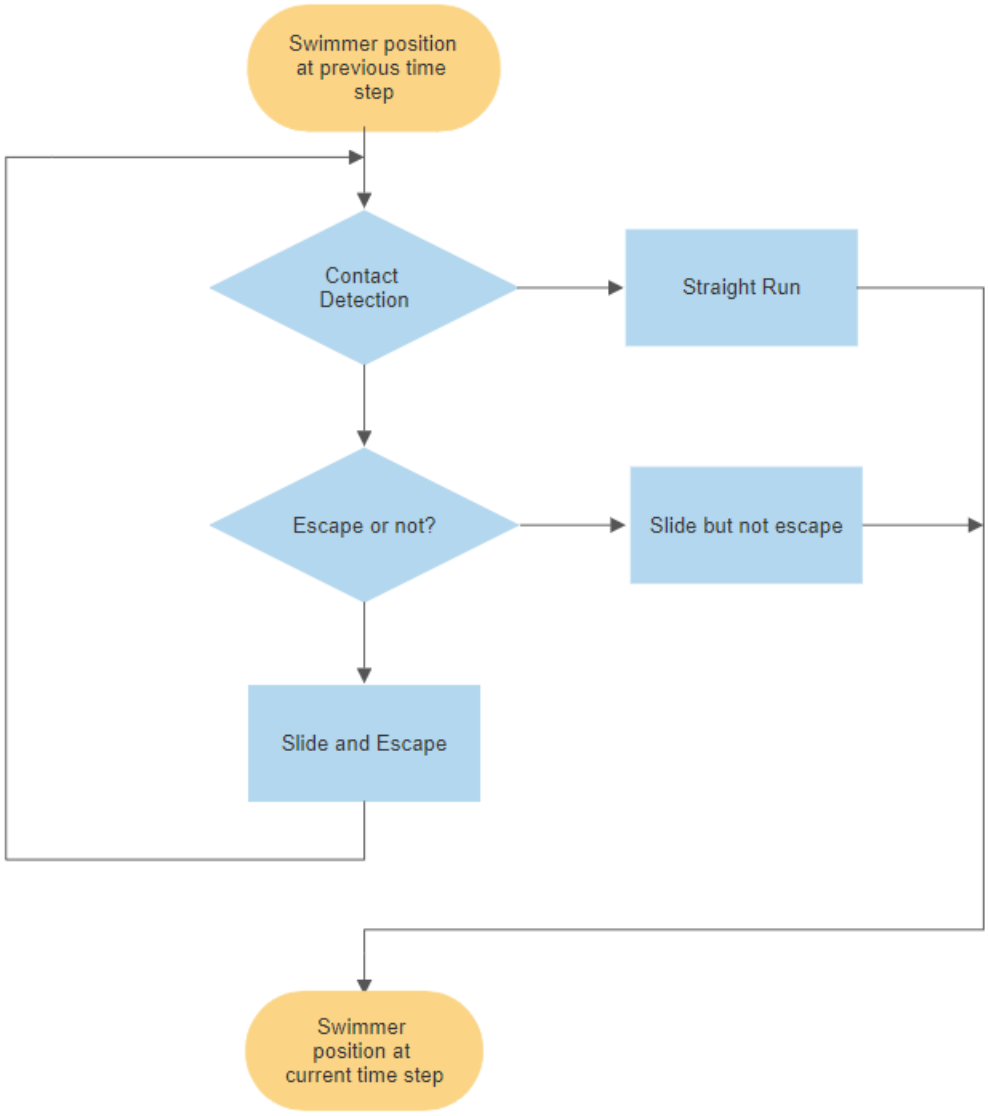

Figure 2.4: Flow chart of the simulation

2.2 2D Domains with Overlapping Pillars

We also consider more complex geometries where the pillar distribution allows pillars to overlap with each other. Therefore, a new pillar will not be removed if it overlaps with an existing pillar: it will only be removed when the new pillar is completely inside an existing pillar. The strategy for analyzing swimmer motion is generally the same as discussed in the section above, but with new complexity induced by the overlapping geometry.

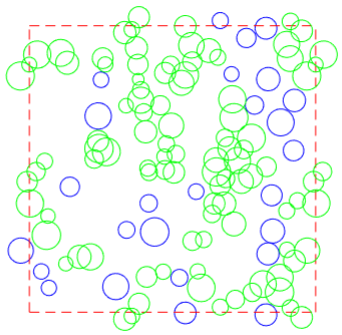

Figure 2.5: Example of configuration that allow pillars to overlap. Circular pillar in blue represents it is not in overlap with any of other pillars, that in green denotes there are at least one pillar overlap with it.

The volume fraction of pillars could be defined in the same way as (2.1.0.1). However, unlike in the non-overlapping case where volume fraction could be computed from direct summation of the area of each pillar, overlapping pillars impose complexity that renders a analytical calculation of the volume fraction difficult. Hence, we perform this calculation numerically. To this end, we discretize the domain into uniformly space cells, where the total number of cells is denoted by N_{total}. If the center of one cell is located inside at least one of the pillars, then that cell should be labelled as "occupied by a pillar". After looping through all the pillars, the number of cells occupied by pillars (N_{inside}) can be counted exactly, and the volume fraction can then be easily computed as:

$$\phi = \frac{N_{inside}}{N_{total}} \tag{2.2.0.1}$$

Obviously, this method will introduce numerical errors, though it is excepted that (2.2.0.1) should converge to the exact volume fraction with mesh refinement. To determine what is the reasonable choice of cell size that balances accuracy and CPU run time, a benchmark testing was implemented by numerically integrating non-overlapping pillars for which the volume fraction is known analytically, as shown in Figure 2.6 and Figure. 2.7. From Figure 2.8, it can be seen that 0.001, for both accuracy and computation efficiency, is a reasonable choice of cell size under which the volume fraction converges.

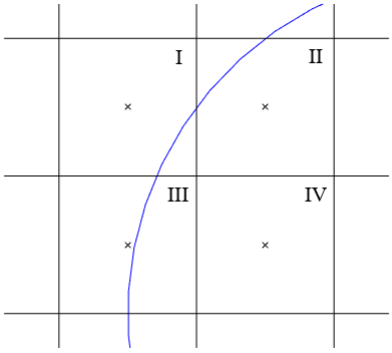

Figure 2.6: Example of discretization. Curve in blue belongs to part of a pillar, black solid lines represent grid cells, and black crosses are the centers of the cells. Cell II and IV are taken to be occupied by a pillar, but I and IV are not.

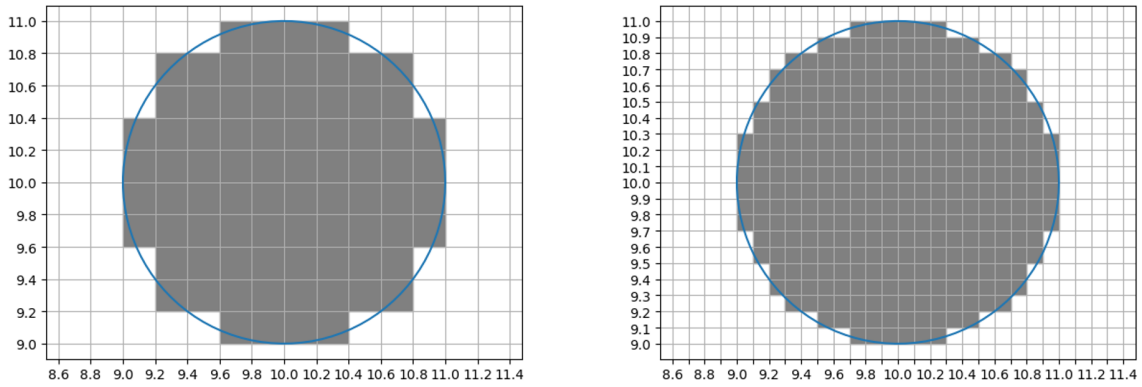

Figure 2.7: Illustration of the numerical integration for one pillar. The domain is discretized by cells with size of 0.2 and 0.1. For this particular pillar, cells marked in grey are labelled as 'occupied' by the pillar.

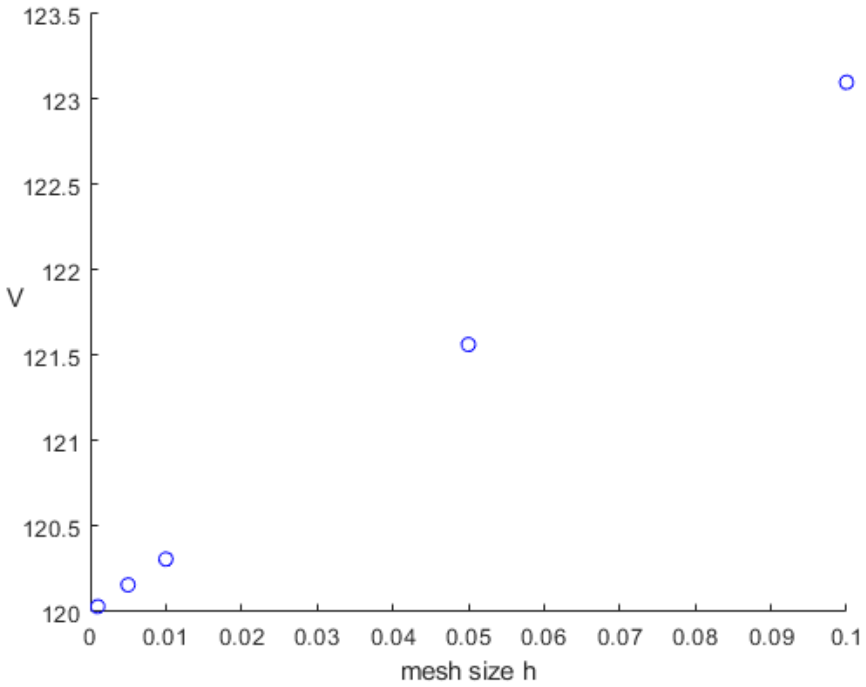

Figure 2.8: Convergence test of the numerical integration. This test is done in a periodic domain filled with non-overlapping pillars with volume fraction of 0.3.

The strategy for the run-and-tumble motion is similar as before, where for each individual run the swimmer undergoes a straight run in the interstice between pillar but slides on pillars

after collision. Consider the case that the swimmer collides with and slides on a pillar. What make overlapping pillars different from non-overlapping pillars is that the swimmer might not finish its run on or escape from the pillar that it first collides with. Scenarios in FIG. ?. (a) and (b) are essentially identical as before: the swimmer will either rest on the pillar at the end of the time step or escape. Assume in the i-th run, run time τ is long enough $\tau \geq t_{escape}$ for swimmer to escape from the pillar that it is colliding with. In this situation, $\boldsymbol{S}_{escape}$ is no longer applicable, since the swimmer will reach the intersection point between the pillar which the swimmer first collided with another pillar, as illustrated in Figure 2.10(c) and Figure 2.10(d). As a result, for the situation where pillar intersections occur before reaching $\boldsymbol{S}_{escape}$, $\boldsymbol{S}_{escape}$ is not applicable anymore; in this case, the nearest intersection point, analog to non-overlapping case, would serve as '$\boldsymbol{S}_{escape}$' to compute 't_{escape}'. Denote '$\boldsymbol{S}_{escape}$' as $\boldsymbol{S}_{inter}$, and the time for swimmer to reach $\boldsymbol{S}_{inter}$ as t_{inter}. It is straightforward to note that $\boldsymbol{S}_{inter}$ is a critical point where swimmer may either continue sliding on the second pillar (Figure 2.10(c)), or get stuck (Figure 2.10(d)).

One pillar can intersect with one or more other pillars, and intersection points can be on either sides of y''. Obviously, intersection points between the pillar that swimmer first collides with and other pillars could be easily obtained by equating two equations for the circles, but one still needs to determine which of two interactions is the closes point to $\boldsymbol{S}_{escape}$. To do this, we define another new coordinate system $(x'O'y')$ with the origin at the collision point, the x axis aligned with swimming direction of the current run, and the y axis obtained by the right hand rule as previously. We transform the coordinates of the intersection points to $x'O'y'$ by $\boldsymbol{S}'_{inter} = \boldsymbol{R}(\boldsymbol{S}_{inter} - \boldsymbol{S}_{collide}$, and the nearest intersection point is the one with smallest positive x' value.

The procedure to determine the time for the swimmer to reach $\boldsymbol{S}_{inter}$ is described as follow. Let α be the initial direction of swimming with the same definition as (2.1.0.2), θ_{inter} be the angle

following (2.1.0.3) that provides information on $\boldsymbol{S}_{inter}$:

$$\theta_{inter} = |Ang\left(\boldsymbol{S}_{inter} - \boldsymbol{P}_{collide}, -\boldsymbol{p}\right)| \tag{2.2.0.2}$$

The time for the swimmer to slide from $\boldsymbol{S}_{collide}$ to $\boldsymbol{S}_{inter}$ is computed by integrating (2.1.0.5) over θ from α to θ_{inter} and t from 0 to t_{inter}:

$$\int_0^{t_{inter}} \frac{2}{d} dt = \int_\alpha^{\theta_{inter}} \frac{1}{|\boldsymbol{v}_0| \sin(\theta)} d\theta$$

$$t_{inter} = \frac{d}{2|\boldsymbol{v}_0|} \log\left(\frac{\cot\alpha + \csc\alpha}{\cot\theta_{inter} + \csc\theta_{inter}}\right) \tag{2.2.0.3}$$

Hence, depending on the remaining run time after collision, the swimmer might complete its run somewhere between $S_{collide}$ and S_{inter} ($t_{remain} \leq t_{inter}$), or overpass S_{inter} ($t_{remain} > t_{inter}$). There is nothing special in the first case: at the next time step, the swimmer will again pick another direction of swimming and run. In the second case, however, the swimmer will either continue sliding or get stuck (Figure 2.10).

Consider the situation where the swimmer collides on the first pillar and reaches S_{inter} before the end of the run. Generally, S_{inter} could belongs to multiple pillars, so which pillar does swimmer continue to slide on? And under which condition will it get stuck? To address the these questions, we first define $\beta \in [0, \pi]$ as the angle between $\boldsymbol{p}$ and $\overrightarrow{O''S_{inter}}$. γ is measured clockwise from $\boldsymbol{p}$ if the y'' component of $\boldsymbol{S}_{inter}$ is positive and anti-clockwise otherwise. From the geometry, we find that the swimmer should slide on the pillar which returns the maximum value of $\gamma < \pi$ among these intersecting pillars (Figure 2.9(a)). Meanwhile, if these exists a pillar for which $\gamma \geq \pi$, then the swimmer will get stuck (Figure 2.9(b)).

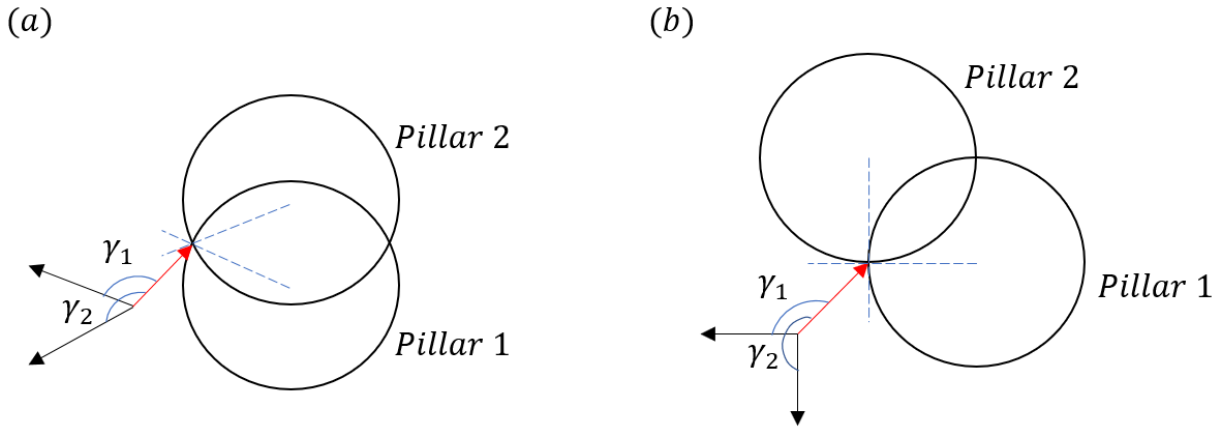

Figure 2.9: (a) $\gamma_1 < \gamma_2 < \pi$, swimmer continue sliding on Pillar2. (b) $\gamma_1 < \pi < \gamma_2$, swimmer get stuck.

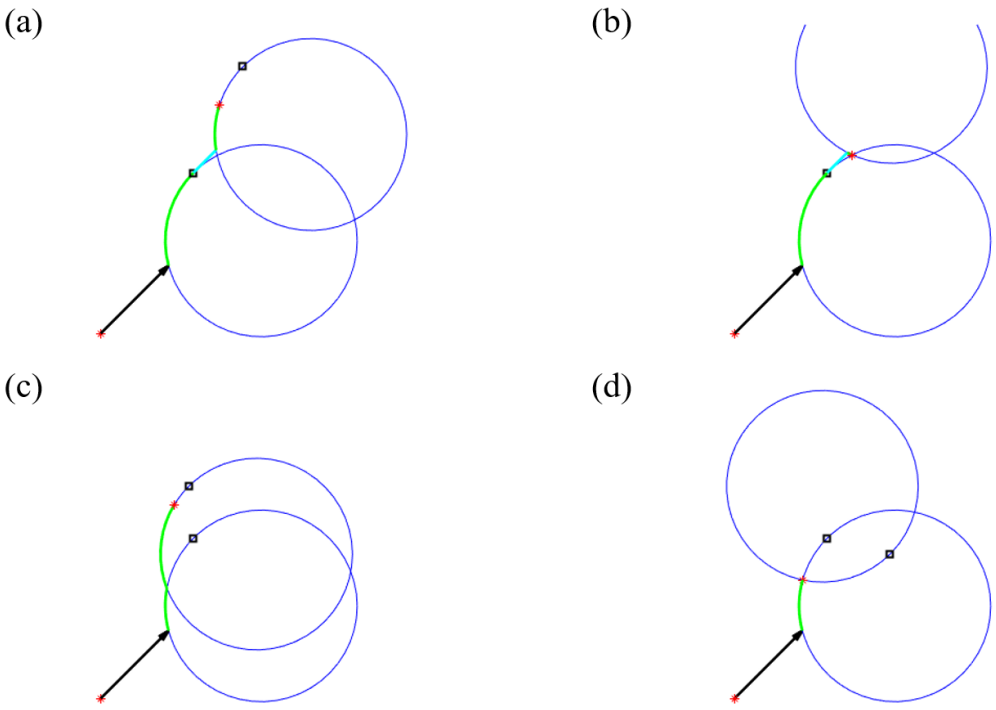

Figure 2.10: (a) S_{escape} is available, swimmer slides on both pillars. (b) S_{escape} is available, but swimmer gets stuck on the second pillar. (c) S_{escape} is unavailable, swimmer slides on both pillars. (d) S_{escape} is unavailable, the swimmer directly gets stuck without sliding.

A flowchart of whole process discussed above is shown in the Figure 2.11 below.

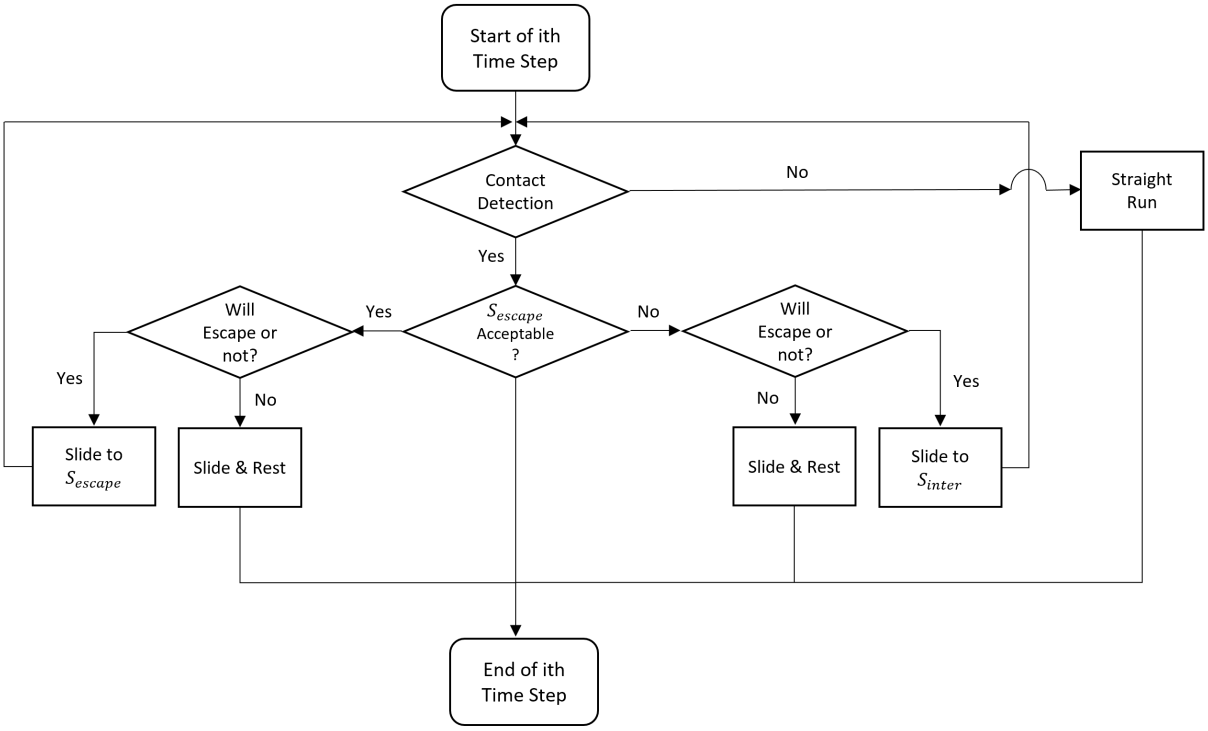

Figure 2.11: Flowchart of the simulation procedures of overlap case.

Chapter 3

Simulation Setup and Results

3.1 Computational Setup

In this Chapter, we provide details of the computational setup, and present and discuss results.

As discussed in Chapter 2, the simulation is conducted inside a periodic box. The reasons for using a periodic box are that swimmers are easier to track, and fewer pillars are required, which reduces the computational cost. Since the objective is to consider the diffusion of swimmers in a domain filled with random obstacles, the periodic boxes should be large enough to contain enough obstacles to capture this randomness. To make sure the domain is representative, a benchmark test was conducted to determine which size of periodic box should be used. In order to compare the effect of periodicity of the domain on the diffusivity, two mostly identical cases are simulated, with the same swimming direction and duration, and a volume fraction of 0.5. The only difference is that one is conducted inside a periodic box with $L = 20$, while the other is simply a large domain without periodicity. The resulting diffusivity shows that there are no differences between these two cases, therefore for the volume fraction of 0.5, $L = 20$ is large enough to capture the randomness of the domain. However, the size of boxes should not be kept constant for various

volume fractions. Consider two cases of volume fraction of 0.1 and 0.5, when reducing it from 0.5 to 0.1, if the box lengths are kept fixed, the total number of pillars contained in the box would also be reduced with the potential for losing some randomness. This problem can be avoided by scaling the size of boxes as we reduce the volume fraction. The scaling factor is determined as follows. Suppose that the length of the box L has been determined for a specific volume fraction, then the expectation of the total number of pillars inside this box is:

$$N = \phi \frac{L^2}{E[d]} \tag{3.1.0.1}$$

where $E[d]$ is the expectation of the pillar diamete, which satisfies uniform distribution with $d \in [d_1, d2]$.

$$E[d] = \int_{d_1}^{d_2} d \frac{1}{d_2 - d_1} dd = \frac{d_1 + d_2}{2}$$

Rearranging (3.1.0.1), we obtain

$$\frac{N}{L^2} = \frac{E[d]}{\phi}$$

N/L^2 can be interpreted as the number density of pillars, which should be kept constant when changing the volume fraction. Hence for another case with volume fraction ϕ', mean pillar diameter $E[d']$ and corresponding box length L', (3.1.0.1) would yield:

$$N' = \phi' \frac{L'^2}{E[d']},$$

$$\frac{N}{L^2} = \frac{N'^2}{L'^2},$$

$$L'^2 = \frac{\phi E[d']}{\phi' E[d]} L^2.$$

Therefore, the scaling factor on the box length is:

$$C = \left(\frac{\phi E[d']}{\phi' E[d]} \right)^{\frac{1}{2}} \tag{3.1.0.2}$$

Since the duration and direction of runs are extracted randomly from the exponential and uniform distributions, respectively, the run-and-tumble dynamics of the swimmers inside the medium is a stochastic process. To obtain the effective diffusivity of the swimmers, their displacements should be averaged over a large enough number of realizations:

$$< \boldsymbol{S}_i >= \frac{1}{N} \sum_{j=1}^{N} \boldsymbol{S}_i \tag{3.1.0.3}$$

Note that since the duration of runs will be different for each realization, the position of the swimmers must be interpolated to the same instant of time to proceed with the averaging in (3.1.0.3). A convergence test for the effect of the number of realizations on the obtained diffusivity was conducted, as shown in 2.8. It can be seen that with increasing number of realizations the diffusivity converges. However, 7000 realizations is computational expensive, so a smaller number of realizations should be used to balance out the computation cost and accuracy of the diffusivity. The value of the diffusivity obtained from 2000 realizations is within 5 percent from that with 7000 realization. In the results shown below, we therefore average over 200 realizations, which provides a balance between computation cost and accuracy. After the average displacements are obtained, a straight line can be fitted to the plot of mean square displacement versus time, whose slope is 4 times the diffusivity in 2D.

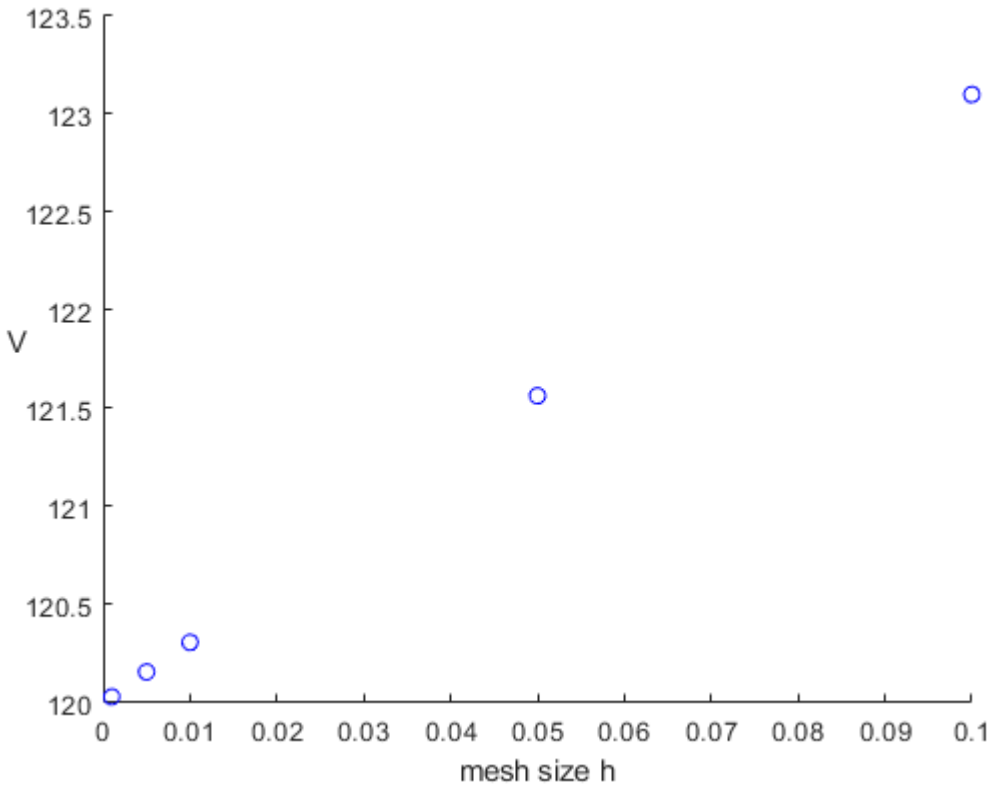

Figure 3.1: Illustration of how effective diffusivity changes with respect to number of realizations.

In terms of the geometry, two dimensionless parameters can be defined to characterize the porous medium. One is the volume fraction which is the ratio between the area occupied by obstacles and the total area of the periodic box. The other one is the ratio between the mean diameter μ of the pillars and its standard deviation σ. For a uniform distribution of pillar size, the probability density function of their sizes is:

$$P(d) = \frac{1}{d_{max} - d_{min}} \tag{3.1.0.4}$$

Then μ, σ and their ratio are given by:

$$\mu = \int_{d_{min}}^{d_{max}} dP(d)dd = \frac{d_{max} + d_{min}}{2}$$

$$\sigma = \int_{d_{min}}^{d_{max}} \left((d-\mu)^2 P(d) dd\right)^2 = \frac{d_{max} - d_{min}}{2\sqrt{3}}$$

$$\frac{\sigma}{\mu} = \frac{1}{\sqrt{3}} \frac{d_{max} - d_{min}}{d_{max} + d_{min}} = C \tag{3.1.0.5}$$

Rearranging (3.1.0.5), we obtain a relation between d_{min} and d_{max}:

$$d_{max} = \frac{1+C}{1-C} d_{min} \tag{3.1.0.6}$$

The volume fraction defines the pillar density inside the domain, with larger volume fractions leading to more frequent collisions with obstacles. In our simulations, we vary the average size μ of the pillars while keeping $\frac{\sigma}{\mu}$ constant, which amounts to keeping the ratio between d_{min} and d_{max} constant. The physical interpretation of that is either placing the same type of swimmer into domains filled with pillars of various diameter ranges, or placing swimmers with different run lengths inside the same domain. Further, since the porous media geometries are also generated randomly, we perform each simulation in five different geometries in order to test whether the diffusivity changes based on pillar arrangement.

3.2 Diffusion in free space: theory

The diffusivity of run-and-tumble swimmers in the free space (no pillars) can be predicted theoretically as follows. Let $\boldsymbol{x}_N$ be the position of swimmer after N runs, $\Delta\boldsymbol{x}_i$ to be the displacement of the swimmer during the i^{th} run. The position of swimmer after N runs is the vector sum of these individual displacements:

$$\boldsymbol{x}_N = \sum_i^N \Delta\boldsymbol{x}_i \tag{3.2.0.1}$$

We assume the displacements during distinct runs are not correlated, and therefore:

$$\begin{aligned} \langle \Delta\boldsymbol{x}_i \cdot \Delta\boldsymbol{x}_j \rangle &= 0 \text{ if } i \neq j \\ \langle \Delta\boldsymbol{x}_i \cdot \Delta\boldsymbol{x}_j \rangle &= (\tau v_0)^2 \text{ if } i = j \end{aligned} \tag{3.2.0.2}$$

where τ is the duration of run which satisfies an exponential distribution, and v_0 is the swimming velocity which is assumed to be constant. Based on (3.2.0.1) and (3.2.0.2), the mean square displacement of the swimmer at step N is:

$$\langle \boldsymbol{x}_i \cdot \boldsymbol{x}_j \rangle = \sum_i^N \sum_j^N (\Delta\boldsymbol{x}_i \cdot \Delta\boldsymbol{x}_j) \tag{3.2.0.3}$$

The probability density function of the run times is given by

$$P(\tau) = \frac{1}{\tau_0} Exp\left(-\frac{\tau}{\tau_0}\right) \tag{3.2.0.4}$$

with mean duration of a run τ_0. The mean square displacement for a single individual step can be expressed as

$$\langle \Delta\boldsymbol{x}_i \cdot \Delta\boldsymbol{x}_j \rangle = \int_0^\infty (\tau v_0)^2 P(\tau) d\tau = 2(\tau_0 v_0)^2 \tag{3.2.0.5}$$

Plugging (3.2.0.5) into (3.2.0.1) gives

$$\langle \boldsymbol{x}_N \cdot \boldsymbol{x}_N \rangle = 2(\tau_0 v_0)^2 N \tag{3.2.0.6}$$

In the limit of long times, we also have $t = N\tau_0$. Therefore, (3.2.0.6) becomes

$$\langle \boldsymbol{x}_N \cdot \boldsymbol{x}_N \rangle = 2\tau_0 v_0^2 t \tag{3.2.0.7}$$

Comparing this with the mean square displacement for Brownian motion in 2D allows us to obtain the diffusion coefficient of run-and-tumble swimmers as:

$$\langle r^2 \rangle = 4Dt$$

$$D = \frac{\tau_0 v_0^2}{2} \tag{3.2.0.8}$$

With non-dimensionalization (using τ_0 as time scale and v_0 as velocity scale), the free space diffusion coefficient is 0.5.

3.3 Results

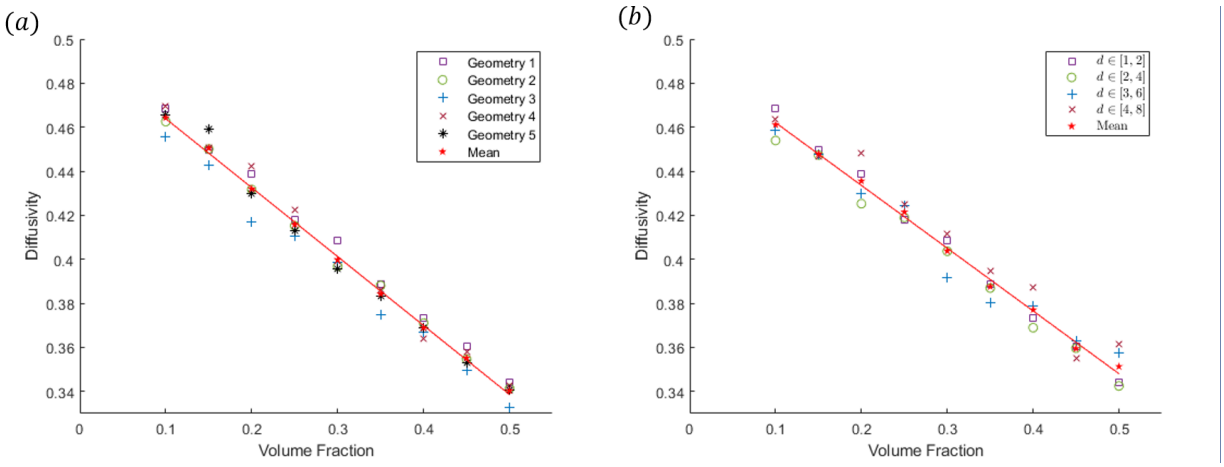

Figure 3.2: (a) Numerically obtained diffusivity as a function of volume fraction and for different random geometries. (b) Diffusivity as a function of volume fraction for different pillar diameter ranges. Both plots are for non-overlapping pillars.

Figure 3.2 illustrates how the long-time diffusivity changes for various volume fractions, random geometries and pillar diameter ranges. From this figure, we see that these exists a small variation between different pillar arrangements, but these variations are generally in the range of 5 percent with respect to the mean value. As shown in both (a) and (b), with the increase of volume fraction, the diffusivity decreases, which is expected as result of collisions with pillars, which reduce transport. The reason of that is straight forward: as the swimmer slides along a pillar, its swimming velocity is the vector projection onto the tangential direction, which reduces the effective magnitude of the velocity. The higher the volume fraction, the larger the possibility for swimmers to collide and slide on pillars, hence the decrease in diffusivity. As can be seen in (a), the red straight line, which is obtained by fitting a straight line only the mean diffusivity for all five geometries, is found to intersect with line of zero volume fraction (vertical axis) at a point around 0.5, which corresponds to the free space diffusivity. The size range of pillars does not have a strong effect on the diffusivity in the non-overlapping pillar case.

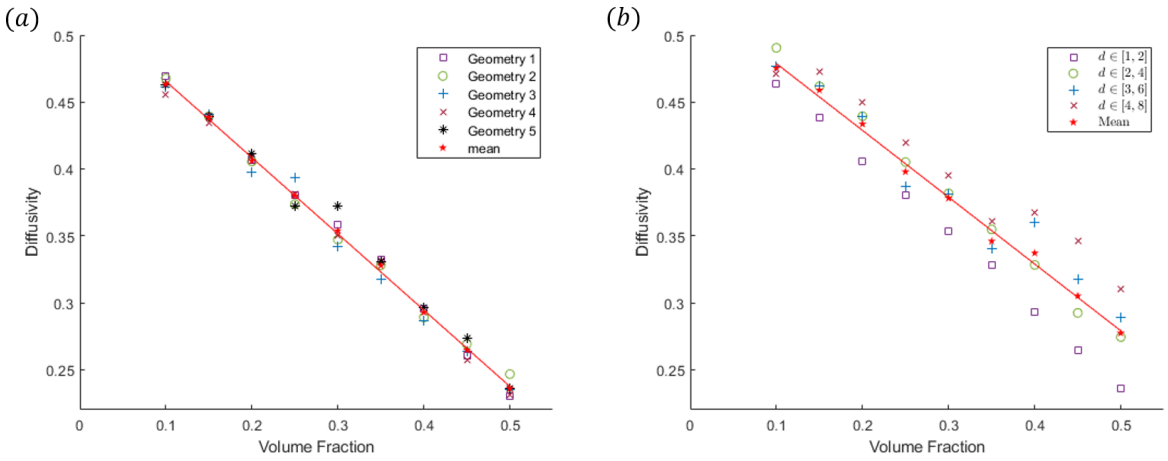

Figure 3.3: (a) Numerically obtained diffusivity as a function of volume fraction and for different random geometries. (b) Diffusivity as a function of volume fraction for different pillar diameter ranges. Both plots are for overlapping pillars.

When pillars are allowed to overlap, the diffusivity also decreases with increasing of volume fraction, but the rate of decrease is larger than that of the non-overlapping case, as shown in 3.3(a). The complexity of the pillar geometry is the root cause for that larger rate of decrease, as swimmers have more possibilities to get stuck compared with the non-overlapping case. Another difference can be seen in 3.3(b), where an increase in pillar size gives rise to a slight increase in diffusivity, as the swimmers spends more time sliding on the pillars when the size of pillars become larger. The time that the swimmer takes to slide from the point of collision to the point where it gets stuck also becomes larger, which decreases the probability for swimmers to get stuck and explains the slight increase in diffusivity in (b).

Chapter 4

Conclusion

In this thesis, the transport of run-and-tumble microswimmers in porous media was modeled numerically. The porous medium is modeled as a periodic box containing circular pillars in two dimensions. The duration of swimmer runs is extracted from an exponential distribution as observed in experiments, while swimming directions during runs are chosen from a uniform distribution of the orientation angle and assumes that orientation of each step is uncorrelated. As the duration of a run is much longer than that of a tumble, we assume in our numerical simulations that tumbles are instantaneous. If the swimmer doesn not collide with any of the obstacles, its trajectory during a run is straight line, as it would be in free space. However, if the swimmer collides with a pillar, it is assumed that the swimmer maintains its orientation and slides on the surface of that pillar with the tangential component of swimming velocity. The swimmer can escape from the pillar as the tangential direction of the pillar surface coincides with the swimming direction. Allowing pillars to overlap introduces complexity in pillar geometry, which modified the escape criteria and add the possibility of swimmers getting stuck in corners: if there exists intersection points between the pillar that the swimmer first collides with and other nearby pillars on the way of sliding to 'S_{escape}', the closest intersection point 'S_{inter}' serves the same role as 'S_{escape}' in non-overlapping case. When it reaches 'S_{inter}', the swimmer will get stuck until the

next tumble if sliding on any of the pillars causes the swimmer to penetrate the other pillar.

Statistics were obtained by averaging trajectories over many realizations. The effective long-time diffusivity of the swimmers in porous media is obtained from the slope of the mean-square displacement vs time. Numerical simulations were conducted for various volume fractions of the porous media and pillar size ranges, for both non-overlapping and overlapping cases. In both cases, the diffusivity was found to decrease with the volume fraction of the pillars, but the complexity of the overlapping geometry leads to a faster decay of the diffusivity with volume fraction. In the non-overlapping case, varying the size the pillars while keeping $\frac{\sigma}{\mu}$ constant does not have any noticeable effect on the diffusivity. However for overlapping case, the diffusivity increases slightly in response to an increase in pillar size.

Bibliography

[1] E. Nelson, *Dynamical Theories of Browian Motion, 2nd Edition*, (Princeton University Press, Princeton, 1967).

[2] H. C. Berg, *Random walks in Biology* (Princeton University Press, Princeton, 1993).

[3] D.J. Acheson, *Elementary Fluid Dynamics* (Clarendon Press, Oxford, 1990).

[4] M E Cates, *Diffusive transport without detailed balance in motile bacteria: does microbiology need statistical physics?*, Reports on Progress in Physics 75, 042601 (2012).

[5] H. C. Berg, *E.coli in motion* (Springer-Verlag, New York, 2004).

[6] C. Bechinger, R. D. Leonardo, H. Lowen, C. Reichhardt, G. Volpe, G. Volpe, *Active particles in complex and crowded environments*, Rev. Mod. Phys, 88, 045006 (2016).

[7] J. Moran and J. Posner, *Microswimmers with no moving parts*, Physics Today 72, 5, 44 (2019).

[8] E.M. Purcell, *Life at Low Reynolds number*, American Journal of Physics, 45, 3 (1997).

[9] G. Taylor, *Analysis of the Swimming of Microscopic Organisms*, Proc. R. Soc. Lond. A 209, 447 (1951).

[10] E. Lauga and T. R. Powers, *The hydrodynamics of swimming microorganisms*,Rep. Prog. Phys. 72, 096601 (2009).

[11] J. Elgeti, R. G. Winkler, and G. Gompper *Physics of Microswimmers - Single Particle Motion and Collective Behavior*

[12] H.C. Flemming and S. Wuertz, *Bacteria and archaea on Earth and their abundance in biofilms*, Nat. Rev. Microbiol 17, 247 (2019).

[13] , R. Cavicchioli, W. J. Ripple, K. N. Timmis et al, *Scientists' warning to humanity: microorganisms and climate change*, Nat. Rev. Microbiol 17, 569 (2019).

[14] S. S. Suarez and A. A. Pacey, *Sperm transport in the femal reproductive tract*, Human Reproduction Update 12, 23 (2006).

[15] O. Osuolala and A. Okoh, *Huamn enteric bacteria and viruses in five wastewater treatment plants in the Eastern Cape, South Africa*

[16] A. L. FLores-Mireles, J. N. Walker, M. Caparon,and S. J. Hultgren, *Urinary tract infections: epidemiology, mechanisms of infection and treatment options*, Nat. Rev. Microbio 13, 269 (2015).

[17] O. Akpor and M. Muchie, *Enviromental and public health implications of wastewater quality*, AFRICAN JOURNAL OF BIOTECHNOLOGY 10, 2379 (2011).

[18] C. Montecucco and R. Rappuoli, *Living dangerously: how Helicobacter pylori survives in the human stomach*, Nat. Rev. Mol. Cell Biol. 2, 457 (2001).

[19] J. Buzhardt and P. Tallapragada *Dynamics of groups of magnetically driven artificial microswimmers*, Phys. Rev. E 100, 033106 (2019).

[20] B. J. Nelson, I. K. kaliakatsos, and J. J. Abbott,]*Microrobots for Minimally Invasive Medicine*, Annual Review of Biomedical Engineering 12, 55 (2010).

[21] R. Dreyfus, J. Baudry, M. L. Roper, M. Fermigier, H. A. Stone, and J. Bibette, *Microscopic artifical swimmers*, Nature 437, 862 (2005).

[22] M. Brun-Cosme-Bruny, E. Bertin, B. Coasne, P. Peyla, and S. Rafai, *Effective diffusivity of microswimmers in a crowded environment*, J. Chem. Phys 150, 104901 (2019).

[23] T. Bhattacharjee and S. S. Datta, *Bactieral hopping and trapping in porous media*, Nat Commun 10, 2075 (20191).

[24] O. Chepizhko and T. Franosch, *Ideal circle microswimmers in crowded media*, Soft Matter 15, 452 (2019).